05

Simulation of subpicosecond laser-plasma X-ray radiation source

© M.V. Sedov[1], S.N. Ryazantsev[1,2], S.A. Pikuz[1,2]

[1] Joint Institute for High Temperatures, Russian Academy of Sciences, Moscow, Russia
[2] National Research Nuclear University „MEPhI", Moscow, Russia

e-mail: sedov_max@mail.ru

Received on December 20, 2021
Revised on December 20, 2021
Accepted on December 30, 2021

The issue of optimizing laser-plasma X-ray sources is still relevant. In this context, numerical simulation methods are very effective. A series of 2d PIC calculations using the EPOCH code were carried out. The laser pulse duration was 0.7 ps, the peak intensity was $3 \cdot 10^{20}$ W/cm^2, and silicon foil between 2 and 5 μm thick was used as a target. The conversion efficiency into the continuous X-ray spectrum was calculated. The results of comparison of numerical calculations with experimental measurements showed their satisfactory agreement.

Keywords: laser plasma, petawatt laser, X-ray radiation, PIC simulation.

DOI: 10.21883/EOS.2022.04.53725.59-21

Introduction

The interaction of a high-intensity laser pulse ($I_L > 10^{18}$ W/cm^2) with a solid-state density target leads to the conversion of significant part of the laser energy (from a few percent to $\sim 50\%$) into relativistic electrons [1–3]). These electrons then propagate deep into the target (or through the secondary target), where part of their energy is transferred either into the continuous X-ray spectrum or into characteristic radiation (through radiative relaxation of the excited states of atoms [3,4]. In this work, plasma radiation is considered exclusively in the continuous X-ray spectrum. Such laser sources can be used for high-resolution X-ray radiography of dense objects [5–9], absorption spectroscopy of heated plasma [7, 8] or for characterizing the distribution of fast electrons [10–14]. In addition, their application for the initiation of photonuclear reactions [15–19] is extremely interesting.

The issue of optimizing such laser-plasmasources of X-ray radiation does not lose its relevance. It should be noted here that plasma radiation into the continuous spectrum is carried out by several mechanisms: bremsstrahlung in collisions of hot electrons with target atoms; radiation arising from the interaction of relativistic electrons with a strong electromagnetic (in particular, laser) field (synchrotron radiation); generation of high harmonics; cyclotron radiation. Note that the scientific literature has not developed a unified terminology for the designation of X-ray radiation arising from the interaction of electrons with a laser field. If the laser pulse is circularly polarized and spins the electrons in a spiral, then the radiation in this case is most often called cyclotron radiation [20,21]. If a laser pulse with linear polarization forces electrons to perform predominantly transverse oscillations (for example, propagating in a plasma channel, or when a thin wire is irradiated), then the resulting X-ray radiation is most often called betatron radiation. If the beam of relativistic electrons is irradiated by laser pulse going towards them, then the resulting radiation is called ?inverse Compton scattering?. In the works [12,13] theoretical estimates for the X-ray emission of electrons in the field of laser pulse, were obtained. In these works, the radiation was called synchrotron radiation, or the term inverse Compton radiation was used as a synonym. In this work, we follow this terminology and use the term synchrotron radiation to describe the X-ray radiation arising from the interaction of relativistic electrons with a strong electromagnetic field. Note that synchrotron radiation can be caused not only by the laser field, but also by strong quasi-static fields that can be induced during the interaction of the laser with the plasma [14].

Cyclotron radiation, in addition to the circularly polarized laser pulse, requires special conditions for spinning electrons in the plasma channel [10] or special targets in the form of nanotubes [11]. Efficient generation of harmonics in the X-ray region also requires special conditions [15]. We consider the interaction of linearly polarized laser pulse with flat target. In this case, the main contribution to the generation of X-ray photons in the continuous spectrum is made by bremsstrahlung and synchrotron radiation. Conducting experimental studies using petawatt-class laser systems is a very costly task; therefore, numerical simulation methods are coming to the fore here. Relatively recently, codes have appeared that allow self-consistently taking into account the X-ray radiation of the plasma in the PIC (particle in cell) calculation: EPOCH [16], OSIRIS [17], CALDER [18], PICLS [19], and others [20], [21]. In the works [22–24], the coefficient of conversion of femtosecond laser pulse into bremsstrahlung and synchrotron radiation was studied for laser intensities$\sim 10^{23}$ W/cm^2. In [20,25] a wide range of laser intensities ($10^{19}-10^{24}$ W/cm^2) was considered. As a result of the study, it was found that the synchrotron radiation begins to exceed the bremsstrahlung at intensity $\sim 10^{22}$ W/cm^2. In the works [26–28], the

angular distribution of photons with energy > 1 MeV as a function of the target thickness for a laser intensity of 10^{23} W/cm^2 [26,28] and for 10^{22} W/cm^2 [27],was studied. Note that all the above works considered a femtosecond laser pulse (30–120 fs). In this paper, X-ray radiation in the continuous spectrum is considered during the interaction of the *p*-field rizovannoth laser radiation (with an intensity of $> 10^{20}$,W/cm^2) sub-picosecond (0.7–1 ps) duration with flat targets of various thicknesses and for various angles of incidence of laser radiation. The simulation results are also compared with experimental measurements obtained at the Vulkan laser facility [22].

Description of numerical calculation

Series of 2d PIC-calculations were performed using the EPOCH code. In this code, bremsstrahlung is simulated using the Monte-Carlo method for elastic and inelastic scattering [29]. Quantum effects, electron-positron-pair production, and synchrotron radiation in the EPOCH code are simulated by quantum electrodynamics methods, also using the Monte-Carlo method [23,24]. The simulation parameters were chosen for maximum agreement with the experiment [22]: the laser pulse had *p*- polarization, the intensity on the target was $3 \cdot 10^{20}$ W/cm^2, laser pulse duration 0.7 ps (0.7–1 ps in the experiment). In the experiment, the diameter of the laser spot was $\sim 7\,\mu$m, the angle of incidence of laser radiation on the target was 45°, the wavelength of laser radiation was 1.054 μm, in calculated for the case of normal incidence, the spot diameter was 4.5 μm, and for the angle of incidence of 45°: $4.5\,[\mu\text{m}]/\cos(\pi/4) \sim 6.4\,\mu$m, wavelength 1 μm. The spatial distribution of the laser pulse was Gaussian, the distribution in time was super-Gaussian of the 3rd- order with a width of 0.7 ps. As a target fully ionized silicon foil of solid density ($5 \cdot 10^{22}$ ions/cm^3) with a thickness of 2 and 5 μm was used; two angles of incidence of the laser pulse on the target were simulated: 0° and 45°. Since the laser pulse in this work has a sub-picosecond duration, it is necessary to set a sufficiently large simulation region in order to correctly describe the interaction of a laser pulse with a rapidly heating and expanding plasma. The modeling area $120 \times 120\,\mu$m evenly divided into cells was used in the calculations. Single cell size is 10×10 nm. To reduce the noise and numerical heating of the plasma, the current smoothing algorithm was used in the calculation, the shape of the macroparticles was prescribed by a 3-spline. At all boundaries, the simulation region is transparent to radiation, and if large particles crossed the boundary, then the code considered that they were reflected from the wall, while their energy became equal to the initial plasma temperature (1 eV).

To save computational time, as well as to better describe the interaction of the laser pulse with the central region of the target, the target was conventionally divided into several zones (Fig. 1): the central zone *1* had 50 large particles-ions

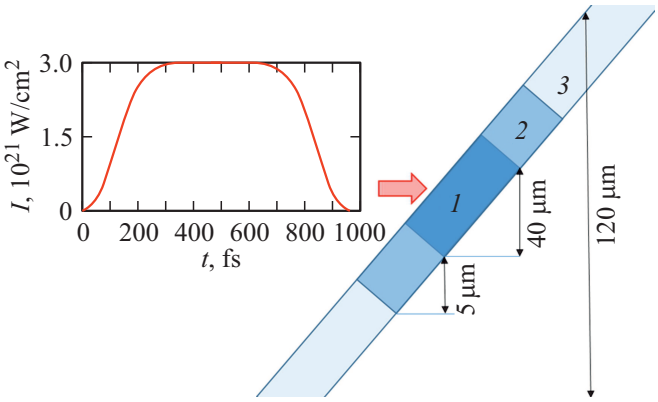

Figure 1. Scheme for numerical simulation.

and 50×14 large particles-electrons in each cell, the *2* zone had half the number of large particles in each cell (25 ions and 25×14 electrons) and zone *3* had 10 large particles-ions and 10×14 large particles-electrons in each cell, respectively. The spatial dimensions of the zones are shown in Fig. 1.

Calculation results

Fig. 2, *a* shows the spectrum of bremsstrahlung and synchrotron radiation for a target with thickness of 2 μm after the end of calculation (900 fs after the laser pulse arrives at the target). Fig. 2, *b* shows the electronic spectrum for the variant with 5 μm-foil and normal incidence of the laser pulse on the target. The spectrum is plotted for different times of interaction of the laser pulse with the target (50–900 fs). Note that due-to the limitation of computing power, we did not simulate the subsequent spread and cooling of the plasma; the calculation ends approximately 50 fs after the end of the interaction of laser pulse with the target. Fig. 3 shows the time dependence of the X-ray yield for different photon energy ranges: 1.7 — 3 keV (*a*), 3–10 keV (*b*), 0.1–1 MeV (*c*) and > 1 MeV (*d*). Fig. 4 shows the integral spatial distribution of the generated X-ray quanta for bremsstrahlung and synchrotron radiation. It should be noted here that in order to save computational resources in the PIC-calculation the passage of X-ray quanta through the target was not simulated. Coordinates, direction of propagation and energy were recorded for the generated photons, then they were removed from the calculation. Absorption was taken into account by a separate post-processing in the process of calculating the conversion coefficient. The dependence of the absorption coefficient on the photon energy was taken from NIST [30] tables.

It can be seen from Figs 2 and 3 that bremsstrahlung dominates in the region of low (< 3 keV) and high (> 1 MeV) energies. In the rest of the spectrum region, the synchrotron radiation dominates. It is also seen from

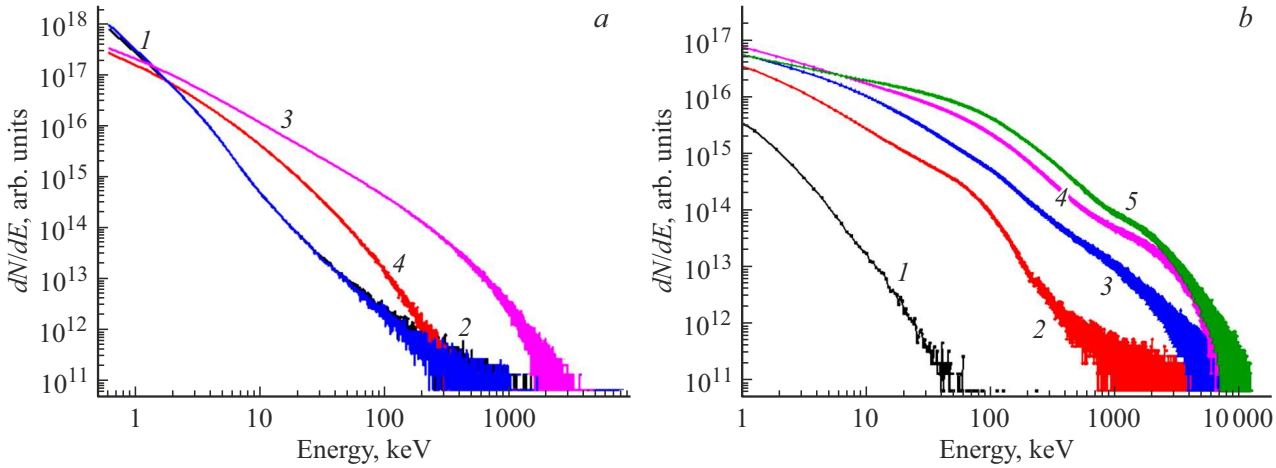

Figure 2. (*a*) Spectrum of bremsstrahlung (blue *1* and black *2* curves) and synchrotron radiation (red *3* and pink *4* curves) for a target 2 *thickmu*m; *1* and *3* is angle of incidence 45°, *2* and *4* is normal incidence. (*b*) Energy distribution function of electrons for different durations of laser pulse interaction with the target: 50 (*1*), 150 (*2*), 250 (*3*), 500 (*4*) and 900 ,fs (*5*); target thickness 5 μm, normal incidence of the laser pulse.

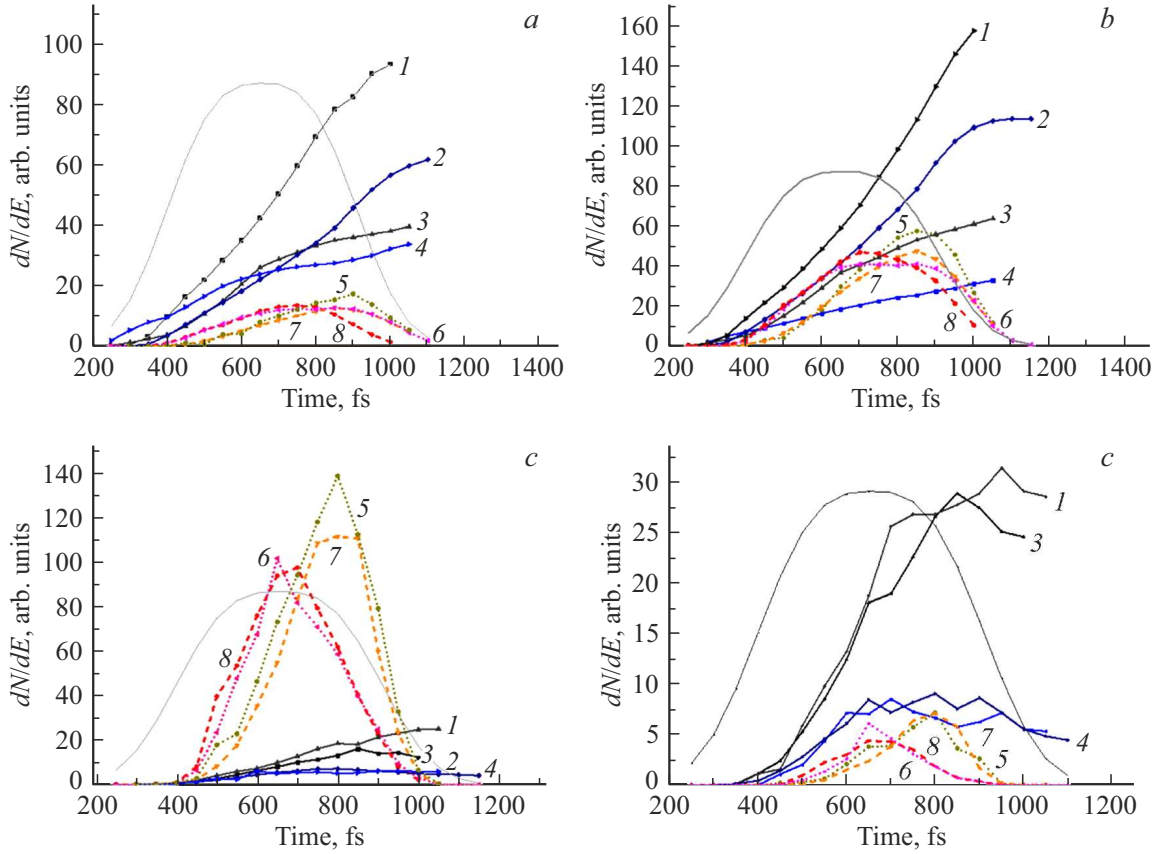

Figure 3. Time dependence of X-ray photon generation for different energy ranges: 1.7−3 keV (*a*), 3−10 keV (*b*), 0.1−1 MeV (*c*) and > 1 MeV (*d*). The solid lines in the figure indicate the dependencies related to bremsstrahlung, the dashed and dotted lines to synchrotron radiation. *1, 2* is bremsstrahlung at an angle of incidence of 45° onto foil with thicknesses of 5 and 2 μm, respectively; *3, 4* is bremsstrahlung at normal incidence on a foil 5 and 2 μm thick; *5, 7* is synchrotron radiation at normal incidence of laser radiation on a foil 2 and 5 μm thick; *6, 8* is synchrotron radiation for an angle of incidence 45° onto a foil 2 and 5 μm thick, respectively.

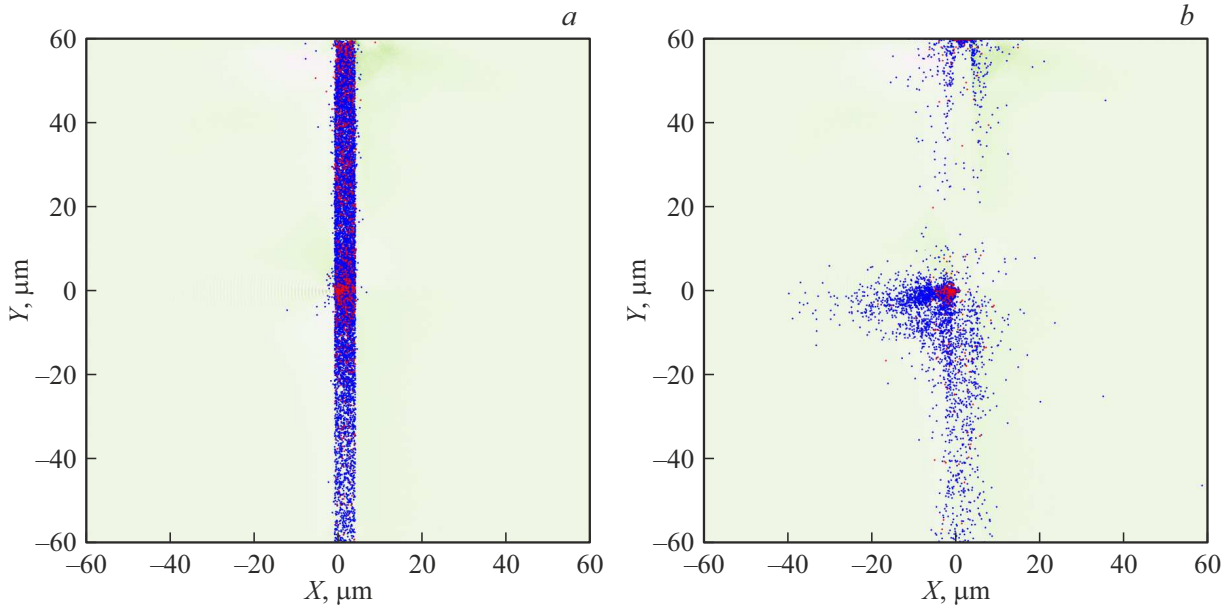

Figure 4. Integral spatial distribution of points of generation of bremsstrahlung (a) and synchrotron (b) quanta up to the end of simulation (1 ps). Red dots designate photons with energies above 1 MeV, blue dots with energies from 0.1 to 1 MeV. Target thickness 5 μm, normal incidence of the laser pulse on the target.

Fig. 3 that the time profile of the synchrotron radiation is approximately two times narrower than the profile of the laser pulse, and the position of the maximum turns out to be dependent on the angle of incidence of the laser radiation on the target: for 45°, the radiation maximum occurs approximately 450 fs after the arrival of the laser pulse on the target, and for normal incidence after ~ 600 fs. Part of this delay (~ 10 fs) is explained by the fact that the laser spot had a diameter of $\sim 3\,\mu$m and at 45° the target inclination angle in the simulation region, the leading edge of the laser pulse reached the target somewhat earlier than in the case of normal incidence. The rest of the time delay, apparently, is explained by the peculiarities of the evolution of the distribution function of hot electrons: efficient generation of synchrotron radiation requires relativistic electrons, and for an angle of incidence of 45°, laser absorption is higher, and relativistic electrons appear earlier in the plasma.

It can be seen from Fig. 3 that the synchrotron radiation is tied to the laser pulse, and as it leaves the target, the generation of synchrotron radiation stops. The efficiency of generation of synchrotron radiation by a plasma electron depends [12,13,23,24] on the quantum parameter η:

$$\eta = \left(\frac{\gamma}{E_s}\right)\left|\mathbf{E}_\perp + \beta \times c\mathbf{B}\right.$$

Here γ is Lorentz factor for electron, E_s is Schwinger field ($E_s = 1.3 \cdot 10^{18}\,\mathrm{V \cdot m^{-1}}$), $\beta = v_e/c$ is electron velocity normalized to velocity light and $\mathbf{E}_\perp$ is electric field strength perpendicular to the electron motion. Thus, generation of synchrotron radiation requires relativistic electrons in a strong electric field perpendicular to their motion and/or in a strong magnetic field. In the case of a flat target, these conditions are satisfied in the focusing region of the laser spot, where major part of the synchrotron radiation is generated (Fig. 4, b). Note that at the edges of the target (top and bottom in Fig. 4, b) there are also regions of synchrotron radiation generation. This is a calculation artifact caused by the influence of boundary conditions. When the action of the laser pulse ends, strong electromagnetic fields on the target quickly disappear, and the generation of synchrotron radiation stops. It can also be seen from Fig. 3 that the synchrotron radiation is practically independent of the target thickness and weakly dependent on the angle of incidence of the laser pulse on the target: at normal incidence, the peak power is approximately 1.3 times higher than at an angle of 45°. This is due to the fact that during normal incidence, the area of the laser spot on the target is $\sqrt{2}$ times smaller, which means that the strength of the laser electromagnetic field is higher; moreover, in this case, the incident laser pulse partially interferes with the reflected one, which also raises the intensity of the laser field [26,27].

The laser pulse generates hot electrons, which then propagate in the target, where they collide with the target atoms and spend part of their energy on generating bremsstrahlung (as well as on ionizing the internal shells of the target, which leads to the generation of characteristic X-rays, but this process we are in this article is not considered). The differential bremsstrahlung cross section in the EPOCH code is implemented as follows [29]:

$$\frac{d\sigma}{dS_\gamma} = \frac{z^2}{\beta^2}\frac{1}{E_\gamma}\chi(Z, E_0, \kappa).$$

Here Z is atomic number of the target material, β is electron velocity normalized to the speed of light, E_0 is electron energy, E_γ is energy of generated bremsstrahlung photon, $\kappa = E_\gamma/E_0$, $\chi(Z, E_0, \kappa)$ is differential scattering cross section, taken from tables, taken from the GEANT 4 [28] code. Accordingly, the bremsstrahlung yield is directly proportional to the square of the target atomic number, target ion density, and the number and energy of hot electrons (in contrast to synchrotron radiation, which directly depends on the intensity of the electromagnetic field). It can be seen from Fig. 3 that the bremsstrahlung intensity strongly depends on the target thickness, especially in the high-energy region (Fig. 3, *d*), for low energies the dependence on the thickness is slightly less pronounced (Fig. 3, *a, b*). This is because the electrons only generate bremsstrahlung photons when they pass through the target. In the simulated case of micron-thick foils, the hottest electrons move almost in a straight line, transit through the target once, and then fly away from the simulation region (or are carried away to the chamber walls in the experiment). Less hot electrons transiting through the target are attracted back by the Coulomb field of the ion core, and their trajectories are a superposition of oscillatory and translational motions along the target [31]. This explains the long afterglow of bremsstrahlung because after the end of the laser pulse, new hot electrons cease to form, but the existing ones continue to circulate over the target. This process is considered in detail, for example, in the works [31,32]. Experimentally measured with the help of X-ray electron-optical cameras with picosecond resolution, the duration of X-ray emission for femto- and picosecond laser pulses is $\sim 3-10$ ps depending on the laser pulse and target parameters [33–36]. Unfortunately, due to limited computing power, we were unable to perform PIC-calculations at times ~ 10 ps in order to accurately depict the smoothly decaying intensity of X-ray bremsstrahlung in Fig. 3. This problem can be circumvented using step-by-step simulation [37,38]: after the end of the interaction of the laser pulse with the target, the energy distribution function of electrons is taken and fed to the input of a numerical code that will calculate the transport of hot electrons through the target and the generation of X-rays. This is planned to be done in a future work.

Table 1–4 shows the coefficient of conversion of laser radiation energy into X-ray quanta in various energy ranges. The first column shows the simulation conditions (target thickness and the angle of incidence of laser radiation on the target), the second column shows the conversion factor for bremsstrahlung after simulation is completed, and the third column shows the conversion factor to synchrotron radiation. Table 1 also shows the experimentally measured conversion rate. Experimental measurements of the absolute yield of X-ray photons were carried out in the range 1.7–3 keV. Laser radiation was incident on the target at an angle of 45°, and silicon foil with a thickness of 2 to 10 μm [22] was used as the target.

Table 1. Conversion coefficient in the range 1.7–3 keV

Conditions simulation	Brake	Synchro-throne	Experiment
0°, 2 μm	$1.2 \cdot 10^{-4}$	$4.0 \cdot 10^{-5}$	
45°, 2 μm	$2.2 \cdot 10^{-4}$	$4.1 \cdot 10^{-5}$	$(7.8 \pm 1.4) \cdot 10^{-4}$
0°, 5 μm	$1.6 \cdot 10^{-4}$	$3.17 \cdot 10^{-5}$	
45°, 5 μm	$3.1 \cdot 10^{-4}$	$3.3 \cdot 10^{-5}$	$(11.2 \pm 0.4) \cdot 10^{-4}$

Table 2. Conversion coefficient in the range 3–10 keV

Conditions of Simulation	Bremsstrahlung	Synchrotron
0°, 2 μm	$1.0 \cdot 10^{-4}$	$1.5 \cdot 10^{-4}$
45°, 2 μm	$3.4 \cdot 10^{-4}$	$1.3 \cdot 10^{-4}$
0°, 5 μm	$1.8 \cdot 10^{-4}$	$1.1 \cdot 10^{-4}$
45°, 5 μm	$3.3 \cdot 10^{-4}$	$1.2 \cdot 10^{-4}$

Table 3. Conversion coefficient in the range of 0.1–1 MeV

Conditions of Simulation	Bremsstrahlung	Synchrotron
0°, 2 μm	$2.0 \cdot 10^{-5}$	$2.8 \cdot 10^{-4}$
45°, 2 μm	$2.5 \cdot 10^{-5}$	$1.8 \cdot 10^{-4}$
0°, 5 μm	$1.2 \cdot 10^{-4}$	$3 \cdot 10^{-4}$
45°, 5 μm	$3.8 \cdot 10^{-5}$	$1.9 \cdot 10^{-4}$

Table 4. Conversion coefficient in the range of > 1 MeV

Conditions of Simulation	Bremsstrahlung	Synchrotron
0°, 2 μm	$1.9 \cdot 10^{-5}$	$1.0 \cdot 10^{-5}$
45°, 2 μm	$2.9 \cdot 10^{-5}$	$0.70 \cdot 10^{-5}$
0°, 5 μm	$9.1 \cdot 10^{-5}$	$0.97 \cdot 10^{-5}$
45°, 5 μm	$7.2 \cdot 10^{-5}$	$0.77 \cdot 10^{-5}$

When comparing the conversion rate with the experimentally measured one, it can be seen that it is about three times less. On the other hand, as mentioned above, bremsstrahlung has a long afterglow ($\sim 3-10$ ps), which was not taken into account in the PIC-race-pair from for limited computing resources. Therefore, obviously, the real conversion factor will be 2–3 times higher, which shows a fairly good agreement with experimental measurements. Comparison of the conversion coefficient found in the PIC-calculation with direct experimental measurements is of great interest because the X-ray calculation module in EPOCH is written primarily for relativistic electrons and photons with energy of > 500 keV. The code can also simulate low-energy photon radiation, but the accuracy of the calculations needs to be verified.

Conclusion

2d PIC-simulation of the interaction of laser radiation with an intensity of $3 \cdot 10^{20}$ W/cm^2 and a flat silicon foil, is carried out. The time dependence of the output of bremsstrahlung and synchrotron radiation is obtained for different energy ranges: 1.7−3 keV, 3−10 keV, 0.1−1 MeV, > 1 MeV. For these spectral ranges, the coefficient of laser pulse energy conversion into X-ray quanta was also determined and compared with the experimentally measured values from the work [22]. Satisfactory agreement between the calculated conversion coefficient for the range 1.7−3 keV and the experimentally measured one is shown.

Acknowledgments

The authors are grateful to S.V. Popruzhenko for help in performing calculations and discussing the results of the study.

Funding

The study was financially supported by the Russian Foundation for Basic Research as part of the scientific project № 19-32-60050, as well as within the state assignment of the JIHT RAS. The calculations were performed on the cluster of RAS Interdeparmental Center for Supercomputing

Conflict of interest

The authors declare that they have no conflict of interest.

References

[1] S.C. Wilks, W.L. Kruer, M. Tabak, A.B. Langdon. Phys. Rev. Lett., **69** (*9*), 1383−1386 (1992). DOI: 10.1103/PhysRevLett.69.1383

[2] A.J. Kemp, F. Fiuza, A. Debayle, T. Johzaki, W.B. Mori, P.K. Patel, Y. Sentoku, L.O. Silva. Nucl. Fusion. **54** (*5*), 054002 (2014). DOI: 10.1088/0029-5515/54/5/054002

[3] K. Yasuike, M.H. Key, S.P. Hatchett, R.A. Snavely, K.B. Wharton. Rev. Sci. Instrum. **72** (*1*), 1236−1240 (2001). DOI: 10.1063/1.1319373

[4] R.B. Stephens, R.A. Snavely, Y. Aglitskiy, F. Amiranoff, C. Andersen, D. Batani, S.D. Baton, T. Cowan, R.R. Freeman, T. Hall, S.P. Hatchett, J.M. Hill, M.H. Key, L.A. King,J.A. Koch, M. Koenig, A.J. MacKinnon, K.L. Lancaster, E. Martinolli, P. Norreys, E. Perelli-Cippo, M. Rabec Le Gloahec, C. Rousseaux, J.J. Santos, F. Scianitti. Phys. Rev. E — Stat. Physics, Plasmas, Fluids, Relat. Interdiscip. Top., **69** (*6*), 7 (2004). DOI: 10.1103/PhysRevE.69.066414

[5] C. Courtois, R. Edwards, A. Compant La Fontaine, C. Aedy, M. Barbotin, S. Bazzoli, L. Biddle, D. Brebion, J.L. Bourgade, D. Drew, M. Fox, M. Gardner, J. Gazave, J.M. Lagrange, O. Landoas, L. Le Dain, E. Lefebvre, D. Mastrosimone, N. Pichoff, G. Pien, M. Ramsay, A. Simons, N. Sircombe, C. Stoeckl, K. Thorp. Phys. Plasmas, **18** (*2*), 023101 (2011). DOI: 10.1063/1.3551738

[6] P. Audebert, P. Renaudin, S. Bastiani-Ceccotti, J.-P. Geindre, C. Chenais-Popovics, S. Tzortzakis, V. Nagels-Silvert, R. Shepherd, I. Matsushima, S. Gary, F. Girard, O. Peyrusse, J.-C. Gauthier. Phys. Rev. Lett., **94** (*2*), 025004 (2005). DOI: 10.1103/PhysRevLett.94.025004.

[7] L. Lecherbourg, P. Renaudin, S. Bastiani-Ceccotti, J.-P. Geindre, C. Blancard, P. Cossé, G. Faussurier, R. Shepherd, P. Audebert. High Energy Density Phys. **3** (*1*), 175−180 (2007). DOI: 10.1016/j.hedp.2007.02.035

[8] F. Pisani, A. Bernardinello, D. Batani, A. Antonicci, E. Martinolli, M. Koenig, L. Gremillet, F. Amiranoff, S. Baton, J. Davies, T. Hall, D. Scott, P. Norreys, A. Djaoui, C. Rousseaux, P. Fews, H. Bandulet, H. Pepin. Phys. Rev. E, **62** (*5*), R5927−R5930 (2000). DOI: 10.1103/PhysRevE.62.R5927

[9] A.L. Meadowcroft, R.D. Edwards. IEEE Trans. Plasma Sci., **40** (*8*), 1992−2001 (2012). DOI: 10.1109/TPS.2012.2201175

[10] H.-P. Schlenvoigt, K. Haupt, A. Debus, F. Budde, O. Jäckel, S. Pfotenhauer, H. Schwoerer, E. Rohwer, J.G. Gallacher, E. Brunetti, R.P. Shanks, S.M. Wiggins, D.A. Jaroszynski. Nat. Phys., **4** (*2*), 130−133 (2008). DOI: 10.1038/nphys811

[11] X. Zhang, T. Tajima, D. Farinella, Y. Shin, G. Mourou, J. Wheeler, P. Taborek, P. Chen, F. Dollar, B. Shen. Phys. Rev. Accel. Beams, **19** (*10*), 101004 2016. DOI: 10.1103/PhysRevAccelBeams.19.101004

[12] F. Mackenroth, A. Di Piazza. Phys. Rev. A, **83** (*3*), 032106 (2011). DOI: 10.1103/PhysRevA.83.032106

[13] A. Di Piazza, K.Z. Hatsagortsyan, C.H. Keitel. Phys. Rev. Lett., **105** (*22*), 220403 (2010). DOI: 10.1103/PhysRevLett.105.220403

[14] D.J. Stark, T. Toncian, A.V. Arefiev. Phys. Rev. Lett., **116** (*18*), 185003 (2016). DOI: 10.1103/PhysRevLett.116.185003

[15] U. Teubner, P. Gibbon. Rev. Mod. Phys., **81** (*2*), 445−479 (2009) DOI: 10.1103/RevModPhys.81.445

[16] T.D. Arber, K. Bennett, C.S. Brady, A. Lawrence-Douglas, M.G. Ramsay, N.J. Sircombe, P. Gillies, R.G. Evans, H. Schmitz, A.R. Bell, C.P. Ridgers. Plasma Phys. Control. Fusion, **57** (*11*), 113001 (2015). DOI: 10.1088/0741-3335/57/11/113001

[17] R.A. Fonseca, S.F. Martins, L.O. Silva, J.W. Tonge, F.S. Tsung, W.B. Mori. Plasma Phys. Control. Fusion, **50** (*12*), 124034 (2008). DOI: 10.1088/0741-3335/50/12/124034

[18] E. Lefebvre, N. Cochet, S. Fritzler, V. Malka, M.-M. Aleonard, J.-F. Chemin, S. Darbon, L. Disdier, J. Faure, A. Fedotoff, O. Landoas, G. Malka, V. Meot, P. Morel, M. Rabec Le Gloahec, A. Rouyer, Ch. Rubbelynck, V. Tikhonchuk, R. Wrobel, P. Audebert, C. Rousseaux. Nucl. Fusion., **43** (*7*), 629−633 (2003). DOI: 10.1088/0029-5515/43/7/317

[19] R. Mishra, P. Leblanc, Y. Sentoku, M.S. Wei, F.N. Beg. Phys. Plasmas., **20** (*7*), 072704 (2013). DOI: 10.1063/1.4812701

[20] F. Wan, C. Lv, M. Jia, H. Sang, B. Xie. Eur. Phys. J. D, **71** (*9*), 236 (2017). DOI: 10.1140/epjd/e2017-70805-7

[21] D. Wu, X. T. He, W. Yu, S. Fritzsche. High Power Laser Sci. Eng., **6**, 50 (2018) DOI: 10.1017/hpl.2018.41

[22] A.S. Martynenko, S.A. Pikuz, I.Yu. Skobelev, S.N. Ryazantsev, C.D. Baird, N. Booth, L.N.K. Döhl, P. Durey, A.Ya. Faenov, D. Farley, R. Kodama, K. Lancaster, P. Mc Kenna, C.D. Murphy, C. Spindloe, T.A. Pikuz, N. Woolsey. Matter Radiat. Extrem., **6** (*1*), 014405 (2021). DOI: 10.1063/5.0025646

[23] R. Duclous, J.G. Kirk, A.R. Bell. Plasma Phys. Control. Fusion, **53** (*1*), 015009 (2011). DOI: 10.1088/0741-3335/53/1/015009

[24] N.V. Elkina, A.M. Fedotov, I.Yu. Kostyukov, M.V. Legkov, N.B. Narozhny, E.N. Nerush, H. Ruhl. Phys. Rev. Spec. Top.-Accel. Beams, **14** (*5*), 054401 (2011). DOI: 10.1103/PhysRevSTAB.14.054401

[25] R.R. Pandit Y. Sentoku. Phys. Plasmas, **19** (*7*), 073304 (2012). DOI: 10.1063/1.4739442.

[26] J.G. Kirk, A.R. Bell, I. Arka. Plasma Phys. Control. Fusion, **51** (*8*), 085008 (2009). DOI: 10.1088/0741-3335/51/8/085008

[27] A.R. Bell, J.G. Kirk. Phys. Rev. Lett., **101** (*20*), 200403 (2008). DOI: 10.1103/PhysRevLett.101.200403

[28] S. Agostinelli, J. Allison, K. Amako, J. Apostolakis, H. Araujo, P. Arce, M. Asai, D. Axen, S. Banerjee, G. Barrand, F. Behner, L. Bellagamba, J. Boudreau, L. Broglia, A. Brunengo, H. Burkhardt, S. Chauvie, J. Chuma, R. Chytracek, G. Cooperman, G. Cosmo, P. Degtyarenko, A.Dell′Acqua, G. Depaola, D. Dietrich, R. Enami, A. Feliciello, C. Ferguson, H. Fesefeldt, G. Folger, F. Foppiano, A. Forti, S. Garelli, S. Giani, R. Giannitrapani, D. Gibin, J.J. Gómez Cadenas, I. González, G. Gracia Abril, G. Greeniaus, W. Greiner, V. Grichine, A. Grossheim, S. Guatelli, P. Gumplinger, R. Hamatsu, K. Hashimoto, H. Hasui, A. Heikkinen, A. Howard, V. Ivanchenko, A. Johnson, F.W. Jones, J. Kallenbach, N. Kanaya, M. Kawabata, Y. Kawabata, M. Kawaguti, S. Kelner, P. Kent, A. Kimura, T. Kodama, R. Kokoulin, M. Kossov, H. Kurashige, E. Lamanna, T. Lampén, V. Lara, V. Lefebure, F. Lei, M. Liendl, W. Lockman, F. Longo, S. Magni, M. Maire, E. Medernach, K. Minamimoto, P. Mora de Freitas, Y. Morita, K. Murakami, M. Nagamatu, R. Nartallo, P. Nieminen, T. Nishimura, K. Ohtsubo, M. Okamura, S. O'Neale, Y. Oohata, K. Paech, J. Perl, A. Pfeiffer, M.G. Pia, F. Ranjard, A. Rybin, S. Sadilov, E. Di Salvo, G. Santin, T. Sasaki, N. Savvas, Y. Sawada, S. Scherer, S. Sei, V. Sirotenko, D. Smith, N. Starkov, H. Stoecker, J. Sulkimo, M. Takahata, S. Tanaka, E. Tcherniaev, E. Safai Tehrani, M. Tropeano, P. Truscott, H. Uno, L. Urban, P. Urban, M. Verderi, A. Walkden, W. Wander, H. Weber, J.P. Wellisch, T. Wenaus, D.C. Williams, D. Wright, T. Yamada, H. Yoshida, D. Zschiesche. Nucl. Instr. Meth. Phys. Res. A, **506** (*3*), 250–303 (2003). DOI: 10.1016/S0168- 9002(03)01368-8

[29] J. Vyskočil, O. Klimo, S. Weber. Plasma Phys. Control. Fusion, **60** (*5*), 054013 (2018). DOI: 10.1088/1361-6587/aab4c3

[30] J.H. Hubbel, S.M. Seltzer. NIST Standard Reference Database, **126**, (2004). DOI: 10.18434/T4D01F

[31] S.N. Andreev, S.G. Garanin, A.A. Rukhadze, V.P. Tarakanov, B.P. Yakutov. Quantum Electron., **40** (*4*), 355–362 (2010). DOI: 10.1070/QE2010v040n04ABEH014272

[32] B. Martinez, E. D'Humières, L. Gremillet. Phys. Rev. Res., **2** (*4*), 043341 (2020). DOI: 10.1103/PhysRevResearch.2.043341

[33] M.M. Murnane, H.C. Kapteyn, R.W. Falcone. Phys. Rev. Lett. **62** (*2*), 155–158 (1989). DOI: 10.1103/PhysRevLett.62.155

[34] F.Y. Khattak, O.A.M.B. Percie du Sert, D. Riley, P.S. Foster, E.J. Divall, C.J. Hooker, A.J. Langley, J. Smith, P. Gibbon. Phys. Rev. E, **74** (*2*), 027401 (2006). DOI: 10.1103/PhysRevE.74.027401

[35] P. Audebert, R. Shepherd, K.B. Fournier, O. Peyrusse, D. Price, R. Lee, P. Springer, J.-C. Gauthier, L. Klein. Phys. Rev. Lett., **89** (26), 265001 (2002). DOI: 10.1103/PhysRevLett.89.265001

[36] O.L. Landen, E.M. Campbell, M.D. Perry, in AIP Conference Proceedings, ed. by M. Lapp, W.C. Stwalley, G.A. Kenny-Wallace (Seattle, WA, USA, 1987), vol. 160, pp. 157–162. DOI: 10.1063/1.36716

[37] J. Limpouch, O. Klimo, V. Bina, S. Kawata. Laser Part. Beams, **22** (*2*), 147–156 (2004). DOI: 10.1017/S0263034604222091

[38] M.V. Sedov, K.Yu. Platonov, A.A. Andreev. Vestnik of SPbGU Fizika i khimiya **4** (62), 23–33 (2017) (in Russian). DOI: 10.21638/11701/spbu04.2017.103 [M.V. Sedov, K.Yu. Platonov, A.A. Andreev. Vestnik SPbSU. Physics and Chemistry, **4** (62), 23–33 (2017). DOI: 10.21638/11701/spbu04.2017.103]